eJSSNT Regular Paper

e-Journal of Surface Science and Nanotechnology **23**, 323–327 (2025)

# Charge States of Ions around Σ5(310)/[001] Grain Boundary in Cubic-$ZrO_2$ Revealed by First-principles Calculations

Shungo Arai,[a] Koji Shimizu,[a, b] Anh Khoa Augustin Lu,[a, c, d] Hiroshi Masuda,[a] Hidehiro Yoshida,[a] Satoshi Watanabe [a, †]

[a] *Department of Materials Engineering, The University of Tokyo, 7-3-1 Hongo, Bunkyo-ku, Tokyo 113-8656, Japan*
[b] *Materials DX Research Center, National Institute of Advanced Industrial Science and Technology (AIST), 1-1-1 Umezono, Tsukuba, Ibaraki 305-8568, Japan*
[c] *Research Center for Materials Nanoarchitectonics (MANA), National Institute for Materials Science (NIMS), 1-1 Namiki, Tsukuba, Ibaraki 305-0044, Japan*
[d] *Mathematics for Advanced Materials Open Innovation Laboratory, National Institute of Advanced Industrial Science and Technology (AIST), 2-1-1 Katahira, Aoba-ku, Sendai, Miyagi 980-8577, Japan*
[†] *Corresponding author: watanabe@cello.t.u-tokyo.ac.jp*

Received: 14 February, 2025; Accepted: 10 July, 2025; J-STAGE Advance Publication: 23 August, 2025; Published: 23 August, 2025

Understanding ion behavior is crucial for advancing the processing of ceramic materials. Given that ion transport predominantly occurs at grain boundaries (GBs) in ceramics, investigating the electronic states in their vicinity is essential. In this study, we perform electronic structure and Born effective charge (BEC) calculations from first principles based on density functional (perturbation) theory, focusing specifically on the Σ5(310)/[001] GB in cubic-$ZrO_2$. Our results reveal the emergence of acceptor states just above the top of the valence band near the GB region. Furthermore, we observe significant deviations in the BECs of both Zr and O near the GB region compared to those in the bulk. These findings suggest the possibility of peculiar ion behavior near GB regions, particularly under applied electric fields.

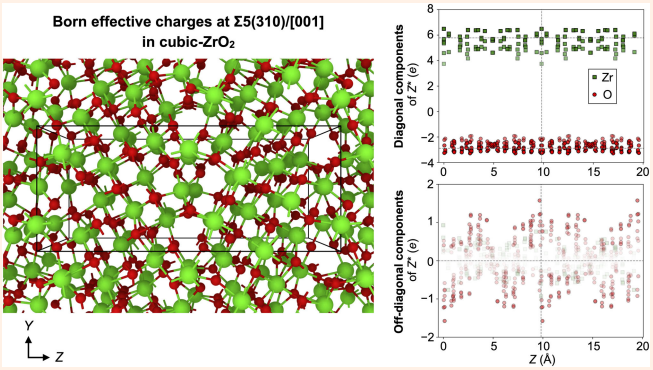


Keywords *$ZrO_2$; Grain boundary; Density functional theory; Density functional perturbation theory; Born effective charge*

## I. INTRODUCTION

Ceramic materials are widely employed across diverse industries owing to their outstanding physical properties, including high heat resistance, wear resistance, and corrosion resistance. Nonetheless, their consolidation process requires compaction of raw powder and subsequent sintering at high temperatures exceeding 1000°C, primarily due to the brittle nature of ceramic materials. This poses significant technical, economic, and environmental challenges. To address these issues, numerous studies have been undertaken to develop more efficient and sustainable processing technologies [1, 2].

To enhance the densification of ceramic powder compacts, various experimental approaches have been explored, including the application of direct or alternating electric fields during sintering [3]. Among these methods, the phenomenon of flash sintering, wherein rapid densification occurs at relatively low temperatures under the influence of strong electric fields, has been observed [4]. Additionally, this phenomenon has been found to facilitate ceramic processing such as high temperature plastic deformation [5] and joining [6]. Although these phenomena are considered to involve enhanced ion transport in the vicinity of grain boundaries (GBs), the fundamental aspects related to them remain elusive, necessitating further elaborate studies using systems that include GBs.

One possible factor that promotes ion transport is the formation of a substantial number of defects in the vicinity of GBs induced by applied electric fields. Several experimental findings support this hypothesis. For instance, it is known that temperature and field strength conditions required for onset of flash event in high-purity alumina can be lowered by doping divalent cations, which would produce oxygen defects [7]. In addition, flash events can enhance fluorescence emission and anelasticity in yttria-stabilized zirconia (YSZ) [8, 9]. These phenomena are explained in terms of the introduction of excessive oxygen vacancies.

As for theoretical study, the ionic behavior at the Σ5(310)/[001] GB in 8 mol% yttria-stabilized zirconia (8YSZ) was examined using classical molecular dynamics (MD) simulations [10]. This study demonstrated an increase in ion diffusivity in response to applied electric fields, influenced by external forces originating from nominal charge states of ions. This phenomenon was ascribed to the formation of vacancies, which led to a reduction in electrostatic potential and space charge near the GB. However, the study did not account for the impacts of polarization resulting from ion displacements and the non-unique allocation of charge density in covalent orbitals. On the other hand, a preceding study by some of the present authors assessed Born effective charges (BECs), which capture the response to external electric fields, in lithium phosphate using density functional perturbation theory (DFPT) [11]. Note that one definition of the BECs, $Z^*_{\alpha\beta}$, is based on the induced atomic forces in response to applied electric fields, which can be calculated using the following formula:

$$Z^*_{\alpha\beta} = \frac{\partial F_\alpha}{\partial E_\beta},$$

where $e$ is the elementary charge, $F_\alpha$ and $E_\beta$ are the atomic forces and the electric field, respectively, and the subscripts $\alpha$ and $\beta$ denote the $X$, $Y$, or $Z$ direction. The preceding study revealed significant variations in charge states of ions depending on their local atomic environment. Notably, anomalous charge states were observed, particularly in the presence of defects, suggesting their possible occurrence near GBs due to the distinct atomic environment compared to the bulk. To the best of our knowledge, BECs at GBs have not been previously investigated. Moreover, ions at GBs are expected to exhibit behaviors distinct from those in bulk crystals under applied electric fields, potentially due to polarization effects arising from atomic misalignment and elemental segregation in the structurally disordered GB region. Alternatively, deviations in charge states from nominal values may lead to enhanced external forces. In the present study, we focused particularly on the latter effect and investigated the electronic states and BECs of GBs in $ZrO_2$.

## II. METHOD

We considered two models. In constructing the first model, we initially modeled a coincidence site lattice GB using the *aimsgb* software [12], based on the cubic-$ZrO_2$ structure

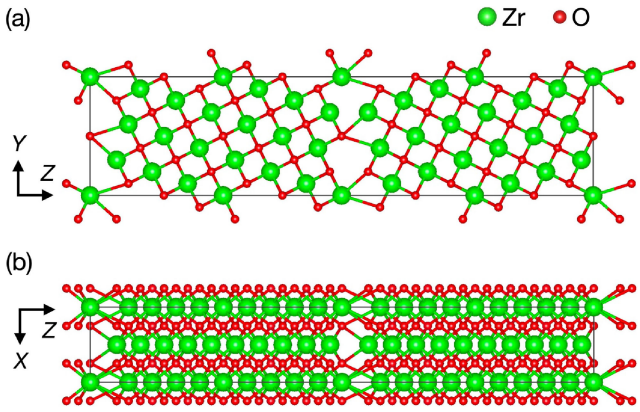


Figure 1: Schematic representations of the first model Σ5(310)/[001] GB in cubic-$ZrO_2$ viewed along (a) *YZ*-plane and (b) *XZ*-planes.

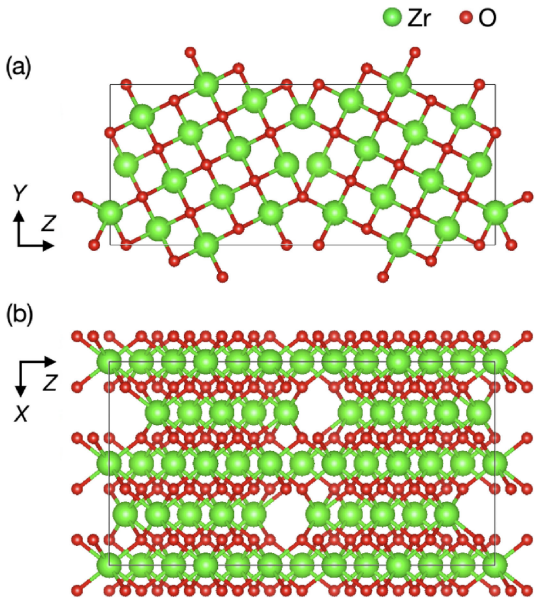


Figure 2: Schematic representations of the second model of Σ5(310)/[001] GB in cubic-$ZrO_2$ viewed along (a) *YZ*-plane and (b) *XZ*-planes.

obtained from the Materials Project database (mp-1565) [13, 14] with lattice constants optimized in this study. Given the considerable computational costs associated with DFPT calculations, we focused on a minimal GB model of Σ5(310)/[001] with a short period of coincidence site lattice. Note that our model contained 120 atoms (40 Zr and 80 O) per supercell in its pristine state. The constructed bi-crystal GB model is depicted in Figure 1, where the GB planes are positioned at the middle and edge of the cell perpendicular to the $Z$-axis. The second model shown in Figure 2 is taken from a previous density functional theory (DFT) study [19]. This model, after structure relaxation, has the lowest energy among the models studied in Ref. 15 and is consistent with a transmission electron microscope observation [16]. This model can be constructed by removing a Zr and two O atoms from a GB (i.e., two Zr and four O atoms in a supercell). The

GB energies of the first and second models calculated with the following computational conditions were 0.0934 and 0.0431 eV Å$^{-2}$, respectively, that is, the second model is more stable. Therefore, we will show and discuss the results on the second model, while those on the first one are included in Supplementary Material.

All DFT and DFPT calculations were performed using the Vienna *Ab initio* Simulation Package (VASP) [17–19]. In these calculations, we used a generalized gradient approximation with the Perdew-Burke-Ernzerhof functional [20], a plane-wave basis set with a 520-eV cutoff energy, self-consistent field convergence criterion of $10^{-5}$ and $10^{-6}$ eV for DFT and DFPT calculations, respectively, and *k*-point sampling mesh of 3 × 4 × 2. Geometry relaxation was performed until the maximum force on atoms fell below 0.02 eV Å$^{-1}$. We optimized the GB structures by adjusting the lattice constant in the *Z*-direction to relieve external pressure. For this purpose, we modified the source code of VASP 6.2.1 to allow geometry relaxation with some lattice parameters fixed. Note that the previous study [15] did not account for such change in the lattice constant in the *Z*-direction.

## III. RESULTS AND DISCUSSION

The optimized structure after relaxation with fixed lattice constants in the *X*- and *Y*-directions and free lattice constants in the *Z*-direction is illustrated in Figure 3, with the corresponding atomic coordinates provided in Table S1 in Supplementary Material. During structural optimization, Zr atoms in the partially depleted Zr columns exhibited displacements toward the GB plane. Although in the previous study, these atoms appeared to lie more directly above the GB plane, the overall displacement trends are qualitatively consistent. The atomic configuration near the GB largely preserves its initial structure; however, noticeable distortions are observed particularly in the oxygen sublattice, which is consistent with the previous report. It should be noted that the method of removing oxygen atoms in our model differs slightly from that inferred from the schematic in the previous study. Nonetheless, our configuration was found to be slightly more energetically favorable and was therefore adopted. As illustrated in Figure S1 (Supplementary Material), the first model exhibits sliding at the GB plane, resulting in more pronounced structural changes at the boundary compared to the second model. Despite this, atomic displacements in regions far from the GB remain minimal.

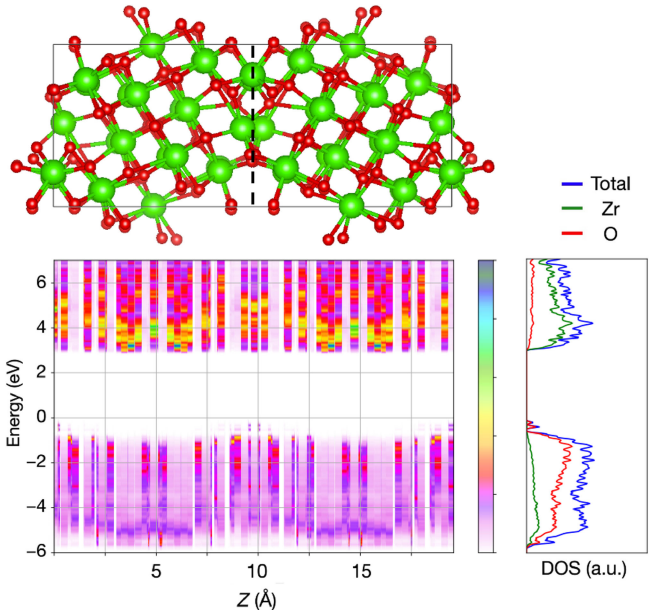


Figure 3: Schematic representation of the optimized Σ5(310)/[001] GB structure in cubic-$ZrO_2$, along with the corresponding DOS and projected DOS along the *Z*-direction, perpendicular to the GB. The energy reference is set to the highest occupied state.

Additionally, we also present the calculated density of states (DOS) for the optimized GB structure in Figure 3. The color map visualizes the projected DOS along the *Z*-axis, with the energy reference set to the highest occupied state. The obtained DOS shows the emergence of unique electronic states near the GB region, distinguishing them from those in areas farther from the GB. Specifically, acceptor energy levels appear just above the valence band around the GB, while no distinct changes are seen in the conduction band. The analysis of the local DOS indicated that the contributions to the valence band top and conduction band bottom were predominantly from O and Zr orbitals, respectively. O orbitals also mainly contribute to the acceptor levels around the GB.

Subsequently, DFPT calculations were conducted to assess the BECs of the optimized GB structure. Figure 4 displays the BEC values of the respective tensor components for the ions along the *Z*-axis. Note that the horizontal dotted lines in the figure denote the BECs of bulk cubic-$ZrO_2$ (with Zr at +5.77e and O at −2.88e). Interestingly, our findings revealed significant deviations in the diagonal components of BECs ($Z^*_{xx}$, $Z^*_{yy}$, and $Z^*_{zz}$) from their bulk values, as depicted in Figure 4(a, e, i). The maximum and minimum BEC values of Zr (O) in the GB structure were +6.49e (−1.91e) and +3.75e (−3.28e), respectively, as summarized in Table 1. In particular, the $Z^*_{yy}$ and $Z^*_{zz}$ components exhibit the most pronounced deviations from the bulk values among the diagonal elements. Additionally, the non-diagonal components of the BEC tensor attain finite and non-negligible values, which is especially evident for oxygen atoms. Zirconium atoms also show finite off-diagonal components.

In cubic crystalline bulk, the off-diagonal components of the BECs were typically zero for both Zr and O ions. However, our calculations revealed finite values for these components. In the vicinity of the GB, this can be attributed to the reduced symmetry, which induces structural anisotropy and results in anomalous off-diagonal BEC values. As shown in Figure 2, atomic displacements are observed throughout the structure, suggesting that the system may have undergone a transition from the ideal cubic phase to a monoclinic-like configuration during structural relaxation. This is plausible, as cubic-$ZrO_2$ is thermodynamically stable only at high temperatures. The monoclinic phase, being inherently ani-

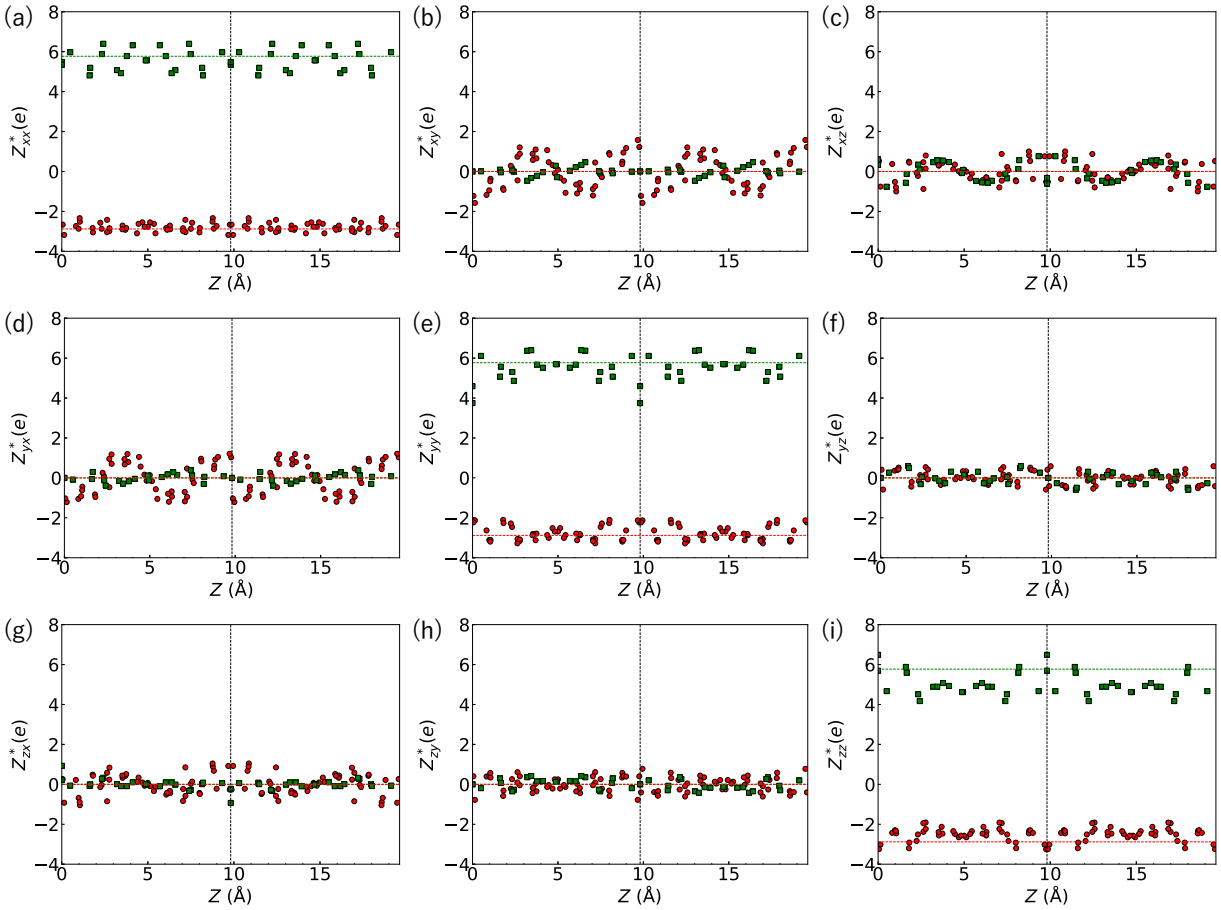


Figure 4: Calculated BECs $Z^*$ for each ion in the Σ5(310)/[001] GB model of cubic-$ZrO_2$. Each tensor component is depicted along the $Z$-direction. Green and red circles denote values of Zr and O, respectively. The vertical dotted lines indicate the boundary between two grains, while the horizontal dotted lines represent the $Z^*$ values of bulk cubic-$ZrO_2$.

Table 1: Maximum and minimum BECs. Parentheses indicate the components of BECs.

| | Diagonal $Z^*$ (e) | | Off-diagonal $Z^*$ (e) | | Bader (e) | |
|---|---|---|---|---|---|---|
| | Max. | Min. | Max. | Min. | Max. | Min. |
| Zr | +6.49 (*zz*) | +3.75 (*yy*) | +0.929 (*zx*) | −0.929 (*zx*) | +2.60 | +2.53 |
| O | −1.91 (*zz*) | −3.28 (*yy*) | 1.58 (*xy*) | −1.58 (*xy*) | −1.23 | −1.32 |

sotropic, naturally exhibits non-zero off-diagonal BEC components. Correspondingly, even the diagonal components of the BEC tensor are expected to differ from those of the cubic phase, given that monoclinic-$ZrO_2$ contains two distinct Zr sites and four distinct O sites. Additionally, the monoclinic phase typically has a lower density than the cubic phase, implying that tensile strain may be introduced in the GB model. Such strain could further amplify the variation and magnitude of the BEC values. It is noteworthy that in the case of our first model, significant deviations from the bulk values were observed mostly in the vicinity of the GB (see Supplementary Material for details). This difference between the first and second models may be attributed to the difference in thickness perpendicular to the GB; the thickness of the second model is only about half of the first model. Since our preliminary calculation on the structural relaxation of the enlarged second model where the thickness perpendicular to the GB was almost doubled exhibited considerable structural change even in the regions far from the GB, which may be due to the fact that the monoclinic phase is the most stable, we remain detailed analysis on the effects of GB on the region far from the GB as a future task. Furthermore, as demonstrated in Ref. 11, under applied electric fields, such non-zero off-diagonal components of the BECs generate external forces perpendicular to the electric field, thereby contributing to enhanced ionic mobilities. Note that these features of the BECs in the GB model are expected to appear regardless of the functional employed, judging from the BEC calculations on monoclinic-$ZrO_2$ (for details, see Supplementary Material). It is also noteworthy that the Bader charges were insensitive to change in local environment compared to the BECs as can be seen in Table 1.

In this way, this study highlights the anomalous variation of BEC values, which depends on the surrounding atomic environment near GBs. Furthermore, under an applied electric field, ions positioned near the GB region are anticipated to experience heightened external forces compared to those

in bulk. Therefore, we shall extend the simulation methods proposed, e.g., in Refs. 11 and 21 to be applicable to GB models in future work, thereby elucidating ion behavior under applied electric fields.

## IV. CONCLUSIONS

In this study, we performed electronic structure and BEC calculations from first principles based on density functional (perturbation) theory, focusing specifically on the Σ5(310)/[001] GB in cubic-$ZrO_2$. Our findings unveil the emergence of acceptor states just above the top of the valence band near the GB region. Furthermore, notable deviations in the BECs of both Zr and O near the GB region compared to those in the bulk were observed. Especially, the off-diagonal components of BECs took finite values for ions near the GB, suggesting the occurrence of forces under applied electric fields in the directions perpendicular to the fields. These findings highlight the distinctive behavior of ions near GB regions, particularly under applied electric fields.

### Acknowledgments

This study was supported by JST CREST Program 'Strong field nanodynamics at grain boundaries and interfaces in ceramics' (JPMJCR1996) and JSPS KAKENHI Grant Numbers (19H02544, 21H05552, 23H04100). Some of the calculations used in this study were performed using the computer facilities at ISSP Supercomputer Center and Information Technology Center, The University of Tokyo.

### Appendix

The atomic coordinate of the optimized pristine GB model, the charge density distributions along the *Z*-axis, and the BECs of $V_O^{2+}$ models are available in Supplementary Material at https://doi.org/10.1380/ejssnt.2025-044.

### Note

This paper was presented at the 10th International Symposium on Surface Science, Kitakyushu International Conference Center, Fukuoka, Japan, 20–24 October, 2024.

## References

[1] M. Yu, S. Grasso, R. Mckinnon, T. Saunders, and M. J. Reece, Adv. Appl. Ceramics **116**, 24 (2017).
[2] C. E. J. Dancer, Mater. Res. Express **3**, 102001 (2016).
[3] R. Raj, M. Cologna, and J. S. C. Francis, J. Am. Ceram. Soc. **94**, 1941 (2011).
[4] M. Cologna, B. Rashkova, and R. Raj, J. Am. Ceram. Soc. **93**, 3556 (2010).
[5] H. Motomura, D. Tamao, K. Nambu, H. Masuda, and H. Yoshida, J. Eur. Ceram. Soc. **42**, 5045 (2022).
[6] K. Nambu, T. Kitaoka, K. Morita, K. Soga, T. Tokunaga, T. Yamamoto, H. Masuda, and H. Yoshida, J. Am. Ceram. Soc. **106**, 2073 (2023).
[7] M. Cologna, J. S. C. Francis, and R. Raj, J. Eur. Ceram. Soc. **31**, 2827 (2011).
[8] Y. Yamashita, T. Kurachi, T. Tokunaga, H. Yoshida, and T. Yamamoto, J. Eur. Ceram. Soc. **40**, 2072 (2020).
[9] H. Masuda, K. Morita, T. Tokunaga, T. Yamamoto, and H. Yoshida, Acta Mater. **227**, 117704 (2022).
[10] W. Xu, A. Maksymenko, S. Hasan, J. J. Meléndez, and E. Olevsky, Acta Mater. **206**, 116596 (2021).
[11] K. Shimizu, R. Otsuka, M. Hara, E. Minamitani, and S. Watanabe, Sci. Technol. Adv. Mater. **3**, 2253135 (2023).
[12] J. Cheng, J. Luo, and K. Yang, Comput. Mater. Sci. **155**, 92 (2018).
[13] The Materials Project provides open web-based access to computed information on various materials properties. http://www.materialsproject.org.
[14] A. Jain, S. P. Ong, G. Hautier, W. Chen, W. D. Richards, S. Dacek, S. Cholia, D. Gunter, D. Skinner, G. Ceder, and K. A. Persson, APL Mater. **1**, 011002 (2013).
[15] Z. Mao, S. B. Sinnott, and E. C. Dickey, J. Am. Ceram. Soc. **85**, 1594 (2002).
[16] E. C. Dickey, X. Fan and S. J. Pennycook, J. Am. Ceram. Soc. **84**, 1361 (2001).
[17] G. Kresse and J. Furthmüller, Comput. Mater. Sci. **6**, 15 (1996).
[18] G. Kresse and J. Furthmüller, Phys. Rev. B **54**, 11169 (1996).
[19] X. Gonze and C. Lee, Phys. Rev. B **55**, 10355 (1997).
[20] J. Perdew, K. Burke, and M. Ernzerhof, Phys. Rev. Lett. **77**, 3865 (1996).
[21] A.-M. El-Sayed, M. B. Watkins, T. Grasser, and A. L. Shluger, Phys. Rev. B **98**, 064102 (2018).

All articles published on e-J. Surf. Sci. Nanotechnol. are licensed under the Creative Commons Attribution 4.0 International (CC BY 4.0). You are free to copy and redistribute articles in any medium or format and also free to remix, transform, and build upon articles for any purpose (including a commercial use) as long as you give appropriate credit to the original source and provide a link to the Creative Commons (CC) license. If you modify the material, you must indicate changes in a proper way.

Copyright: ©2025 The author(s)
Published by The Japan Society of Vacuum and Surface Science